

## Estimation of musculoskeletal models from *in situ* measurements of muscle action in the rat hindlimb

Sang Hoon Yeo<sup>1</sup>, Christopher H. Mullens<sup>2,3</sup>, Thomas G. Sandercock<sup>2</sup>, Dinesh K. Pai<sup>1</sup>  
 and Matthew C. Tresch<sup>2,4,5,\*</sup>

<sup>1</sup>Department of Computer Science, University of British Columbia, Vancouver, British Columbia, Canada, <sup>2</sup>Department of Physiology, <sup>3</sup>Northwestern University Interdepartmental Neuroscience Program, <sup>4</sup>Department of Biomedical Engineering and <sup>5</sup>Department of Physical Medicine and Rehabilitation, Northwestern University, Chicago, Illinois 60611, USA

\*Author for correspondence (m-tresch@northwestern.edu)

Accepted 21 October 2010

### SUMMARY

Musculoskeletal models are often created by making detailed anatomical measurements of muscle properties. These measurements can then be used to determine the parameters of canonical models of muscle action. We describe here a complementary approach for developing and validating muscle models, using *in situ* measurements of muscle actions. We characterized the actions of two rat hindlimb muscles: the gracilis posticus (GRp) and the posterior head of biceps femoris (BFp; excluding the anterior head with vertebral origin). The GRp is a relatively simple muscle, with a circumscribed origin and insertion. The BFp is more complex, with an insertion distributed along the tibia. We measured the six-dimensional isometric forces and moments at the ankle evoked from stimulating each muscle at a range of limb configurations. The variation of forces and moments across the workspace provides a succinct characterization of muscle action. We then used this data to create a simple muscle model with a single point insertion and origin. The model parameters were optimized to best explain the observed force–moment data. This model explained the relatively simple muscle, GRp, very well ( $R^2 > 0.85$ ). Surprisingly, this simple model was also able to explain the action of the BFp, despite its greater complexity ( $R^2 > 0.84$ ). We then compared the actions observed here with those predicted using recently published anatomical measurements. Although the forces and moments predicted for the GRp were very similar to those observed here, the predictions for the BFp differed. These results show the potential utility of the approach described here for the development and refinement of musculoskeletal models based on *in situ* measurements of muscle actions.

Key words: muscle model, biceps femoris, moment arm.

### INTRODUCTION

Although studies of biological motor control often focus on the strategies implemented by neural systems, the properties of peripheral systems – the skeleton, muscles, tendons, connective tissue, etc. – also make significant contributions to the production of movement. In many cases these peripheral systems have been shown to simplify neural control or make natural behaviors more efficient (Nishikawa et al., 2007; Pfeifer et al., 2007; Valero-Cuevas et al., 2007b). Any understanding of the neural control of movement, therefore, clearly requires an understanding of the peripheral musculoskeletal systems with which it interacts.

Such an understanding of peripheral systems is commonly formalized in computational musculoskeletal models (e.g. Delp and Loan, 1995; Sueda et al., 2008; Teran et al., 2003; Valero-Cuevas, 2009). Musculoskeletal models have been used in many different contexts and have been helpful in gaining insights into biological motor control. Although there are a wide variety of musculoskeletal models used in the literature, in general these models are created from ‘the bottom up’: investigators make a large number of independent measurements of physiological parameters (e.g. optimal muscle length, physiological cross-sectional area, moment arms, etc.) which are then used to specify a model of muscle action (Brown and Loeb, 2000; Burkholder and Nichols, 2004; Holzbaaur et al., 2005; Johnson et al., 2008; Kargo et al., 2002; Kargo and Rome, 2002; McKay et al., 2007; Topp and Rosen, 1990). Such reductionist

approaches are very appealing because they provide a standardized way to construct musculoskeletal models across a wide range of species, and measured parameters are usually directly related to well-defined muscle properties.

Although this approach to developing musculoskeletal models has been generally successful, there are several issues concerning this approach that are often difficult to evaluate. At a basic level, the validity of such models can be difficult to establish: the measurement of muscle parameters is subject to error and this error can result in a range of estimated muscle actions (Santos et al., 2009; Santos and Valero-Cuevas, 2003; Valero-Cuevas et al., 2003). One crucial property of muscles included in such models is their moment arm. In muscles that are represented as line segments, the moment arm of a muscle depends on its origin and insertion. However, many muscles have a broad insertion and/or origin. If a muscle is represented with a single origin and insertion to define its line of action, it is not always obvious, based on anatomical dissection, where to best place these points. Furthermore, it is not always clear what degree of model complexity is necessary to capture muscle action. For instance, to model especially complex muscles with very broad insertions or origins, investigators often divide the muscle into several distinct regions, modeling each region with an independent insertion and origin which together span the observed muscle anatomy (Chadwick et al., 2008; Holzbaaur et al., 2005). How to divide these complex muscles into distinct regions and the most

appropriate location of their respective insertion and origin points is not usually obvious.

The present study develops and evaluates an approach that can potentially help guide and validate the development of musculoskeletal models. We take an integrative approach to modeling the actions of individual muscles, using 'top down' empirical characterizations of measured muscle actions to create parameterized muscle models. This approach is an extension of that developed by Loeb et al. (Loeb et al., 2000) and is related to other work attempting to estimate muscle moment arms by direct measurement of muscle action (Lee et al., 2008; Pearlman et al., 2004; Valero-Cuevas et al., 2000). In particular, we measured, *in situ*, the forces and moments produced by stimulation of individual muscles in the rat hindlimb. These forces and moments are a direct consequence of the intrinsic force-generating properties of a muscle working through its attachment to the skeleton (Loeb et al., 2000). Any muscle model attempting to characterize the action of a muscle should therefore be able to predict these forces and moments well. In addition, because these measurements are closely linked to the properties of the stimulated muscle, it should be possible to estimate the parameters for a muscle model (i.e. its anatomical origin and insertion and its intrinsic force-generating properties) based on the forces and moments observed experimentally. The present study took this approach, using the experimentally observed forces and moments to create a parameterized muscle model to capture the action of muscles.

We applied this approach to two different muscles in the rat hindlimb, the gracilis posticus and the biceps femoris (Greene, 1935). The gracilis posticus is a relatively simple, band-like muscle with well-defined origin and insertion. We expected that this muscle would be well described with a model consisting of a single insertion and origin. In contrast, the biceps femoris is a complex muscle with an insertion distributed across the tibia from the knee to the ankle (Gillis and Biewener, 2001). Given this complex insertion, it is not obvious where one should place the insertion of this muscle on the tibia, or whether multiple insertions might be required to describe the action of this muscle. We expected that this muscle would be poorly described by a single insertion and origin and would require a more complex model structure to capture its action (Valero-Cuevas et al., 2007a). These two muscles, representing a range from simple to complex muscle architectures allowed us to evaluate the utility of our approach for the development and validation of muscle models.

A preliminary report of these experiments and analyses was previously published as a conference proceeding (Tresch et al., 2010).

## MATERIALS AND METHODS

### Experimental preparation

Data was obtained from five adult female rats (*Ratus norvegicus* Berkenhaut 1769; mass 250–300 g). All procedures were approved by the Institutional Animal Care and Use Committee at Northwestern University. Rats were anesthetized with ketamine and xylazine (80 and 10 g kg<sup>-1</sup>; intraperitoneally). Metal posts were attached to three points on the pelvis using bone screws and cement: one each, on the rostral and caudal ends of the contralateral (right) pelvis and another on the rostral end of the ipsilateral pelvis (Fig. 1A). A threaded attachment was then cemented to bone screws attached at the distal tibia so that it was approximately perpendicular to the tibia. The anterior head of gracilis was severed and gently peeled back to expose the nerve innervating the posterior head of gracilis. The nerve was gently freed from the surrounding tissue and a small

cuff electrode with bipolar exposed leads was placed around the nerve, insulated with Vaseline, and secured to surrounding tissue using cyanoacrylic glue. To prepare the biceps femoris (BF) for stimulation, the anterior head of the biceps femoris (BFa) was first severed close to its origin on the vertebrae and partially removed by gently cutting its adhesion to the posterior portion of the biceps (BFp). BFp here refers to the entire region of the BF, which has an origin on the ischium and inserts along the extent of the tibia (see Discussion). We then exposed the branch of the tibial nerve innervating the BFp by cutting the gluteus maximus and caudofemoralis, then peeling back the caudofemoralis to expose the nerve. The branch of the nerve to the semimembranosus was cut; the remaining nerve was freed from surrounding tissue, placed in a cuff electrode, insulated with Vaseline, and secured to the surrounding tissue.

We then separated the semitendinosus from the BF, cutting through the connections between the two muscles and severing the semitendinosus distal to the fusion of its medial and lateral heads. Exposed muscles were covered with moist gauze. Finally, we performed a dorsal laminectomy to expose the lumbar spinal cord and dorsal roots. The L4 and L5 ipsilateral dorsal roots could be visually identified by their size and, after opening the dura and applying a few drops of lidocaine to the cord surface, the ipsilateral dorsal roots from L1 to L6 were severed. We usually also cut a dorsal root rostral and caudal to the identified roots in order to ensure full deafferentation of the limb. The deafferentation was confirmed during the experiments by observing a lack of response to a strong pinch of the ipsilateral foot while observing a response to a similar pinch applied to the contralateral foot used to assess anesthetic state.

The animal was then transferred to the experimental setup and positioned (Fig. 1A). The posts cemented to the pelvis were attached to magnetic stands anchored to the table surface so that the pelvis was approximately level in medial–lateral and anterior–posterior directions. The threaded rod in the distal tibia was attached to a six-axis force transducer (Mini40; ATI, Apex, NC, USA). The transducer was mounted on a series of stages, which allowed it to be moved along the dorsoventral, mediolateral and rostrocaudal axes of the rat. Once the limb was attached to the transducer the only possible movement at the ankle was a rotation around the mediolateral axis. This rotation could be prevented or permitted by set screws. The ankle was positioned so that it was approximately in the same mediolateral plane as the hip center. The temperature of the rat was monitored with a rectal thermometer and maintained between 37 and 39°C using a heat lamp placed above the animal. Fluids were given to the animal immediately after the initial surgical preparation (dextrose 3 ml subcutaneously) and in between collections of force field data sets (approximately every 3 h).

### Experimental protocol and data collection

We first determined recruitment curves for individual muscles, varying the current level and measuring the change in evoked force. Stimulation trains (75 Hz, 0.2 ms pulses, 500–1000 ms duration) were applied through the implanted cuff electrodes in order to evoke a muscle contraction with the limb fixed at a specific configuration in the workspace. The forces and moments measured by the transducer were collected (2000 Hz) using custom software in Labview for a period of 1 s before and 3 s after the stimulation train onset.

Stimulation trains were applied at a fixed interval of 1 min. Current was increased gradually from the threshold response until the evoked peak magnitude reached a plateau level. We measured the response for several current levels above the plateau level as

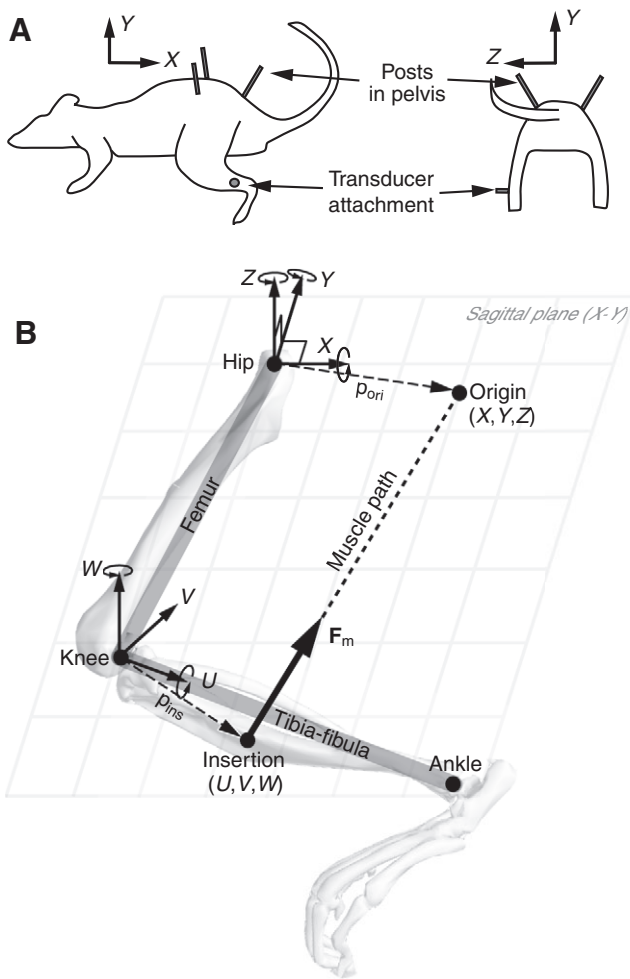


Fig. 1. (A) Experimental setup. The pelvis was immobilized by three posts: one in the rostral and one in the caudal end of the contralateral pelvis and one in the rostral end of the ipsilateral pelvis. A six-dimensional force and moment transducer was secured to an attachment cemented to the distal tibia on the left hindlimb. In this configuration, the X-, Y- and Z-axes are aligned with the rostral-caudal, dorsal-ventral and medial-lateral directions, respectively. (B) Kinematic structure and coordinate frames defined for the hindlimb. The origin of the muscle is defined as a point (X, Y, Z) in a coordinate frame with an origin at the hip, and the insertion is defined as a point (U, V, W) in a coordinate frame fixed to the tibia-fibula with an origin at the knee. Skeletal geometry is modeled as a two-link serial chain, where the hip joint is modeled as a ball joint (X–Y–Z rotation) fixed to the ground (pelvis) and the knee joint is modeled as a universal joint (U–W rotation). The overlaid skeleton is shown to help visualize the coordinate frames. Fig. 1A is modified with permission from Tresch and Bizzi (Tresch and Bizzi, 1999).

well, making sure that the evoked force was not altered, in order to ensure lack of current spread to adjacent muscles. From these recruitment curves, we chose a current level that evoked a maximal activation of the muscle (between 0.06 and 0.45 mA). Once the current level was established, we then measured how the evoked forces and moments varied across the hindlimb workspace. The limb was fixed in a configuration, the muscle stimulated and the evoked forces and moments measured at the ankle with the attached force transducer. Two types of trials were collected for each muscle at a single limb configuration. In one trial, all degrees of freedom at the ankle were restrained (by securing the set screws;

referred to as ‘restrained’ trials). In the other trial, rotation about the mediolateral axis of the ankle was permitted (by releasing the set screws; referred to as ‘released’ trials). By visual inspection, any such rotations were generally very small during evoked responses. Stimulation trains to any muscle were applied at an interval of 1 min. After collecting the evoked responses at a single limb configuration, the ankle was moved to a new position. We took care not to move the limb to the extremes of the workspace to avoid kinematic singularities or overstretching muscles. Stimulation was then applied to each muscle at the new position, for both restrained and released conditions. For each animal, 19–24 limb configurations were measured in order to span a range of limb configurations throughout the hindlimb workspace. Periodically through the collection of these responses the limb was returned to the original configuration and stimulation repeated to evaluate the effects of fatigue on the evoked responses. At the end of the experiment, the animal was killed by pentobarbital overdose and the position of the hip center of rotation was measured and the limb was dissected to find the distance from the hip to the knee center of rotation and the distance between the knee center of rotation and the rod attached to the foot. The mediolateral distance from the origin of the force transducer to the center of the foot was also measured for each animal in order to set the tool transform for the collected forces and moments.

#### Data analysis and modeling

We examined only the active force produced by each muscle, obtained by subtracting the averaged forces and moments measured prior to the onset of each stimulation train. We then found the peak force produced by each muscle and extracted the six-dimensional vector of peak forces and moments at each position. The set of these six-dimensional vectors measured at each limb configuration comprises a ‘force–moment field’ similar to the force fields that have been used previously (Giszter et al., 1993; Loeb et al., 2000). As described above, these fields are the result of the intrinsic force-generating properties of each muscle acting through the attachment of the muscle to the skeleton. In the approach described here we attempted to find a model of muscle action that is capable of explaining the observed muscle actions.

#### Parameterized muscle model

We characterized the muscle by two parameters: maximal force (peak tetanic tension) and optimal muscle length. Note that we did not include an extra parameter for tendon length in these models. Although this parameter is in general necessary to account for the difference between musculotendon length and muscle fascicle length, including this extra parameter did not substantially improve the quality of the fits described here. Moreover, as long as the muscles acts predominantly upon the ascending portion of the force–length functions (see Fig. 8), the parameters of maximal force, optimum length and tendon slack length have redundant effects on the predicted muscle force for the isometric measurements made here. For fully activated muscle, we approximated the relationship between muscle length and force magnitude with a Gaussian curve with standard deviation (s.d.) equal to  $0.2 \times$  muscle length:

$$\mathbf{F}_m = f_{\max} \exp\left(-\frac{(l/l_0 - 1)^2}{2(0.2)^2}\right) \mathbf{u}, \quad (1)$$

where  $f_{\max}$  is the maximal force,  $l$  is the muscle length,  $l_0$  is the optimal muscle length, and  $\mathbf{u}$  is a unit vector from the insertion to



the original point of the muscle. The force produced by the muscle acts through its attachment points on the skeleton. In this study we considered each muscle to have a point origin and insertion. Each point could be an arbitrary position in three-dimensional space, with the insertion described in a local frame attached to the tibia–fibula. Thus, the action of each muscle was characterized by eight parameters, three for the origin, three for the insertion, the optimal length and the maximal force.

#### Kinematic model of the rat hindlimb

As shown in Fig. 1B, we modeled the rat hindlimb as a two-link serial chain consisting of the femur and tibia–fibula. The foot was omitted from analyses because we were concerned with muscles acting on the proximal joints. The hip was modeled as a ball joint and the knee was modeled as a universal joint with motion in flexion–extension in the sagittal plane and motion in pronation–supination of the tibia–fibula. There were thus five degrees of freedom in the limb. Constant centers of rotation were used for both the hip and knee joints.

#### Relating muscle force to forces and moments at the ankle

To predict forces and moments measured at the ankle for a given muscle force, we used standard methods from robotics based on Jacobians to translate between coordinate frames (Murray et al., 1994). In our study, a Jacobian is a matrix representing the linear map from joint angular velocities to the ankle velocity. Using the transpose of the Jacobian matrix, we can relate the force produced by the muscle to the ankle forces and moments by relating both to their equivalent joint torques. Relating muscle force to joint torques, we have:

$$\boldsymbol{\tau}_m = J_m^T \mathbf{F}_m, \quad (2)$$

where  $\mathbf{F}_m$  is a  $(3 \times 1)$  vector of forces applied to the insertion point by the muscle,  $J_m$  is the  $(3 \times 5)$  Jacobian matrix relating muscle force to joint torques and  $\boldsymbol{\tau}_m$  is the  $(5 \times 1)$  vector of joint torques created by the muscle force. Similarly, we can relate joint torques to the endpoint force:

$$\boldsymbol{\tau}_a = J_a^T \boldsymbol{\Psi}_a, \quad (3)$$

where  $\boldsymbol{\Psi}_a$  is the  $(6 \times 1)$  vector of forces and moments measured at the ankle,  $J_a$  is the  $(6 \times 5)$  Jacobian matrix relating muscle force and moments measured at the ankle to joint torques and  $\boldsymbol{\tau}_a$  is the  $(5 \times 1)$  vector of joint torques needed to produce  $\boldsymbol{\Psi}_a$  at the endpoint.  $J_a$  and  $J_m$  were calculated using standard formulations of the Jacobian based on a rigid body analysis.  $J_a$ ,  $J_m$  and  $\mathbf{F}_m$  vary with the configuration of the limb. When the limb is in equilibrium, the torques must balance, as can be described by the equation:

$$J_a^T \boldsymbol{\Psi}_a = J_m^T \mathbf{F}_m. \quad (4)$$

If one considers the configuration of these experiments, it can be seen that there is a mismatch in the number of degrees of freedom within the hindlimb (five) and the measured forces and moments (six). Because of this, when the ankle was completely restrained by fixing the rotation around the mediolateral axis, the limb was overconstrained by the attachment to the force transducer. In such a situation, translating between intrinsic forces produced by the muscle and the forces and moments measured by the force transducer is not a well-posed problem, i.e. in general, there is not a unique mapping between the two sets of forces although the physical system has a unique mapping, dictated by the intrinsic stiffness of the force transducer and hindlimb (Mussa-Ivaldi and Hogan, 1991).

Mathematically, this problem can be described as finding  $\boldsymbol{\Psi}_a$  in Eqn 4 for a given  $J_a$ ,  $J_m$  and  $\mathbf{F}_m$ . Note that because  $J_a$  is not square it cannot be inverted, so that although transforming ankle forces and moments into joint torques is well defined, the mapping from joint torques to ankle forces and moments is not. In order to translate between intrinsic muscle force and endpoint forces and moments, we therefore formed the Moore–Penrose (M–P) pseudoinverse (Golub and van Loan, 1996) of  $J_a$ , and used it to predict the forces and moments at the ankle that result from contraction of the muscle:

$$\boldsymbol{\Psi}_a = J_a (J_a^T J_a)^{-1} \boldsymbol{\tau} = J_a (J_a^T J_a)^{-1} J_m^T \mathbf{F}_m. \quad (5)$$

The M–P pseudoinverse is similar to the standard matrix inverse in that  $J_a^T \boldsymbol{\Psi}_a$  gives  $\boldsymbol{\tau}$  back, as can be easily seen from Eqn 5. Of the many possible values of  $\boldsymbol{\Psi}_a$ , Eqn 5 picks the one with the smallest magnitude: i.e. the least squares inverse of the matrix. However, this solution does not necessarily correspond to the true mechanical solution determined by the stiffnesses of the system and other pseudoinverses are also possible (Mussa-Ivaldi and Hogan, 1991). One important issue in considering M–P pseudoinverses is that the solution satisfying the least squares criterion depends on the choice of units used in the measurements. In our case,  $\boldsymbol{\Psi}_a$  consists of both forces and moments, which have different units. This is a well-known issue in robotics [e.g. appendix A, section 3.2 in Murray et al. (Murray et al., 1994)], for which there is a simple and standard solution, which is to choose an appropriate length scale to compare rotational quantities and translational quantities. In our case, the length scale is based on the size of the limb. We carefully chose units (newtons for forces and newton centimeters for moments) to make sure that both types of properties have similar orders of magnitude. Further, we verified that the results were minimally affected by changing the relative weight between two units within a reasonable range. However, because of these issues of the indeterminacy of the pseudoinverse, we compared this approach with a complementary one in which a pseudoinverse was not necessary.

In the second approach, referred to here as the ‘released’ method, we used the trials in which the rotational degree of freedom around the mediolateral axis was released (the ‘released’ trials described above). If this degree of freedom is released and we assume that as a consequence when the limb is at rest there are no moments generated about this mediolateral axis, then the five degrees of freedom of the limb are matched with the five degrees of freedom measured by the force transducer. In this situation,  $\boldsymbol{\Psi}_a$  is reduced to a five-dimensional vector  $\tilde{\boldsymbol{\Psi}}_a$  (three forces and two moments) and we can define a reduced  $(5 \times 5)$  Jacobian  $\tilde{J}_a$  by removing the row from  $J_a$  corresponding to the rotation along the released axis. Because  $\tilde{J}_a$  is square and thus invertible,  $\tilde{\boldsymbol{\Psi}}_a$  can be uniquely determined as follows:

$$\tilde{\boldsymbol{\Psi}}_a = (\tilde{J}_a^T)^{-1} \boldsymbol{\tau} = (\tilde{J}_a^T)^{-1} J_m^T \mathbf{F}_m. \quad (6)$$

Releasing this degree of freedom makes moments around this axis to be zero, but, in principle, it may cause the forces and moments measured along the remaining restrained degrees of freedom to differ from those measured with the limb fully restrained. However, we found that the forces and moments were only minimally altered when this degree of freedom was released (see Results).

#### Parameteric optimization

We found the set of muscle model parameters that best predicted the force–moment fields measured at the ankle, minimizing the error between observed and predicted force–moment fields. If forces and

moments were measured at  $N$  limb configurations, the optimization problem can be defined as:

$$\min_{\mathbf{d}} \sum_{i=1}^N \|\boldsymbol{\psi}_i - \hat{\boldsymbol{\psi}}_i(\mathbf{d})\|^2, \quad (7)$$

where  $\mathbf{d}$  is the eight-dimensional vector of muscle model parameters and  $\hat{\boldsymbol{\psi}}_i(\mathbf{d})$  is the ankle and force moments predicted for the  $i$ th configuration.  $\hat{\boldsymbol{\psi}}_i(\mathbf{d})$  is the predicted action of the muscle from either the restrained or released analyses described in the previous section, and  $\boldsymbol{\psi}_i$  is the data taken from either the restrained or released trials. The set of parameters that minimized this error was found using lsqnonlin in Matlab. The optimization routine was started with reasonable guesses for the initial parameters, with the origin placed caudal to the hip center and the insertion placed near the tibia–fibula. We also tried different initial guesses and found that the result was robust to the selection of initial guesses.

A concern in fitting any model is whether the identified model overfits the data, explaining noise in the data rather than the structural variation. We therefore performed an  $n$ -fold cross validation. Each force field was divided into five sets of positions, chosen randomly. One set of positions was set aside and the remaining four sets were used to find model parameters, using the optimizations described above. We then evaluated the prediction of the identified model over the set of positions which were set aside. This procedure was repeated for each of the five sets of positions.

#### Evaluating fit quality

To quantify the quality of the fit to the observed data, we used a centered  $R^2$  computed as one minus the ratio between the residual error variance in the model and the total variance of the data. An  $R^2$  value near one indicates that there is minimal residual error,

whereas an  $R^2$  near zero indicates that the model performs the same as the mean of the data. Note that this is a conservative measure of fit quality in the present case, because predicting the mean force produced by the muscle is non-trivial but is a result of the specific origins and insertions found by the optimization.

#### Comparison with existing muscle models

Johnson et al. (Johnson et al., 2008) report a comprehensive musculoskeletal model for the rat hindlimb based on detailed anatomical measurements. We used these data plus the muscle architecture data of Eng et al. as the basis of a forward model to compute the force–moment fields in the present study (Eng et al., 2008). Johnson et al.'s variable joint center data, femur and tibia lengths, and muscle origin and insertion locations were incorporated in the model. This model will be referred to in this manuscript as the Johnson parameter model (Johnson et al., 2008). [Note that Johnson et al. have updated the model in SimTK, which is available online at the SimTK website ([https://simtk.org/home/rat\\_hlimb\\_model](https://simtk.org/home/rat_hlimb_model)) to include wrapping surfaces, made slight changes in some parameters, and the most recent model version considers the knee to move in only flexion extension. In the predictions shown here we used the model parameters and structure as described in Johnson et al. (Johnson et al., 2008).] As with our method above, the model has five degrees of freedom:  $X$ ,  $Y$ ,  $Z$  rotations for the hip joint and  $U$ ,  $W$  rotations for the knee joint (see Fig. 1). To approximate the experimental conditions, we assumed that the knee was in the same mediolateral plane as the ankle (see the figures). Using the femur and tibia lengths from Johnson et al., we found the corresponding joint angles, allowing for the variable joint centers described by Johnson et al. These five angles were used to position the skeleton and determine the origin and insertion of the BFP and the gracilis posticus (GRp). Ankle force and moments were calculated using

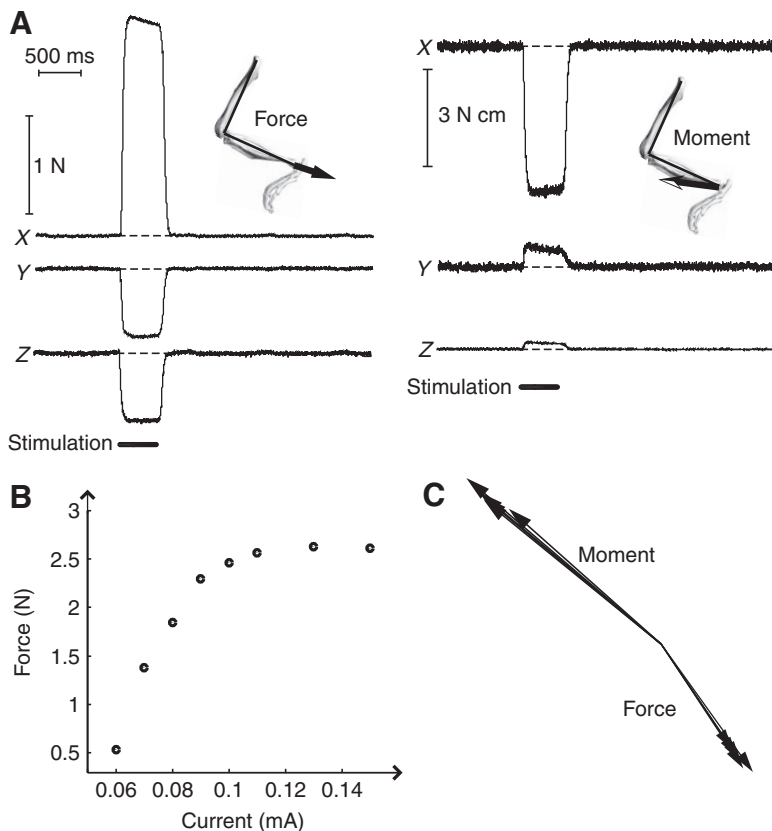


Fig. 2. Force and moments evoked by *in situ* muscle stimulation in the rat hindlimb. (A) Recorded forces and moments evoked by stimulation of the posterior head of biceps femoris (BFP) for one trial. Force and moment quickly reached plateau levels at the onset of the stimulation and returned to baseline levels after the end of the stimulation. (B) Magnitudes of the evoked force of biceps femoris across a range of current levels. As the current level increases, the force reached a plateau level (around 0.13 mA) and did not increase further, suggesting that the muscle was maximally activated after 0.13 mA. (C) Variation of evoked force and moment by biceps femoris in the same limb configuration across five repeated trials, separated by 8, 12, 12 and 14 min.

Eqn 4.  $J_a$  and  $J_m$  were determined numerically from the Johnson parameters for each set of joint angles. Because in the Johnson et al. manuscript joint centers are a function of joint angle,  $J_a$  and  $J_m$  as calculated here are slightly different from the analytic calculations used above. The magnitude of  $f_m$  was determined using a force-length relationship based on the data of Eng et al. (Eng et al., 2008). The shape of the function was approximated using an idealized sarcomere force-length function (Gordon et al., 1966) corrected for actin length in the rat (Rassier et al., 1999). The width of the function was scaled by muscle fiber length. The optimal length was set to muscle length. The maximal force was based on physiological cross-sectional area multiplied by  $22 \text{ N cm}^{-2}$ .

## RESULTS

### Forces and moments evoked by *in situ* stimulation of rat hindlimb muscles

Fig. 2A shows an example of the forces and moments evoked from stimulation of the biceps femoris at a single limb configuration. As seen in the trial, the evoked response quickly reached a plateau level, which was sustained for the duration of the stimulation train then returned to the prestimulation baseline levels. Fig. 2B shows an example of the variation in the evoked force magnitude with the current level used to activate the nerve. In this example, the magnitude reached a plateau at 0.13 mA. Further increases of current past this level did not result in increases in the evoked force magnitude, suggesting that the muscle was maximally active. Fig. 2C shows the force and moment vectors in the  $X$ - $Y$  plane taken at the time of peak response for the trial shown in Fig. 2A. We have separated the plots of forces and moments in order to make them easier to see, although in the data analyses and development of muscle models described below they were combined in a single six-dimensional vector. We also show the force and moment vectors evoked on repeated trials during the collection of a single force field in Fig. 2C. The vectors were collected at intervals of 8, 12, 12 and 14 min. The similarity of these vectors demonstrates the consistency of muscle stimulation in these experiments, although there is also fatigue over time because of the many trials of stimulation used here. Taken together, the results shown in Fig. 2 (see also Figs 3 and 4) demonstrate the reliability of the experimental preparation and collected data to characterize muscle actions.

### Force and moment fields produced by stimulation of the GRp and Bfp

Fig. 3 shows the force and moment fields evoked by stimulation of the GRp for each of the five animals, with the ankle movement fully restrained. The equivalent fields for the Bfp are shown in Fig. 4. GRp produced a set of forces that drove the limb caudally, dorsally and medially. Fig. 3 shows that the force and moment fields measured for the GRp were very consistent across animals. Fig. 5A shows an example of two force and moment fields measured for one animal, either with the ankle fully restrained or with rotation around the mediolateral axis released. As can be seen in the figure, the moments around the mediolateral axis were minimal when the rotation was permitted while other degrees of freedom were only minimally affected.

Although the forces and moments measured for the GRp were generally consistent with what might be expected from the anatomy of this muscle (see below), the responses measured for the Bfp were less expected. Although Fig. 4 shows that the responses evoked by stimulation of the Bfp were similar across animals, the evoked forces were directed caudally in extension with only a

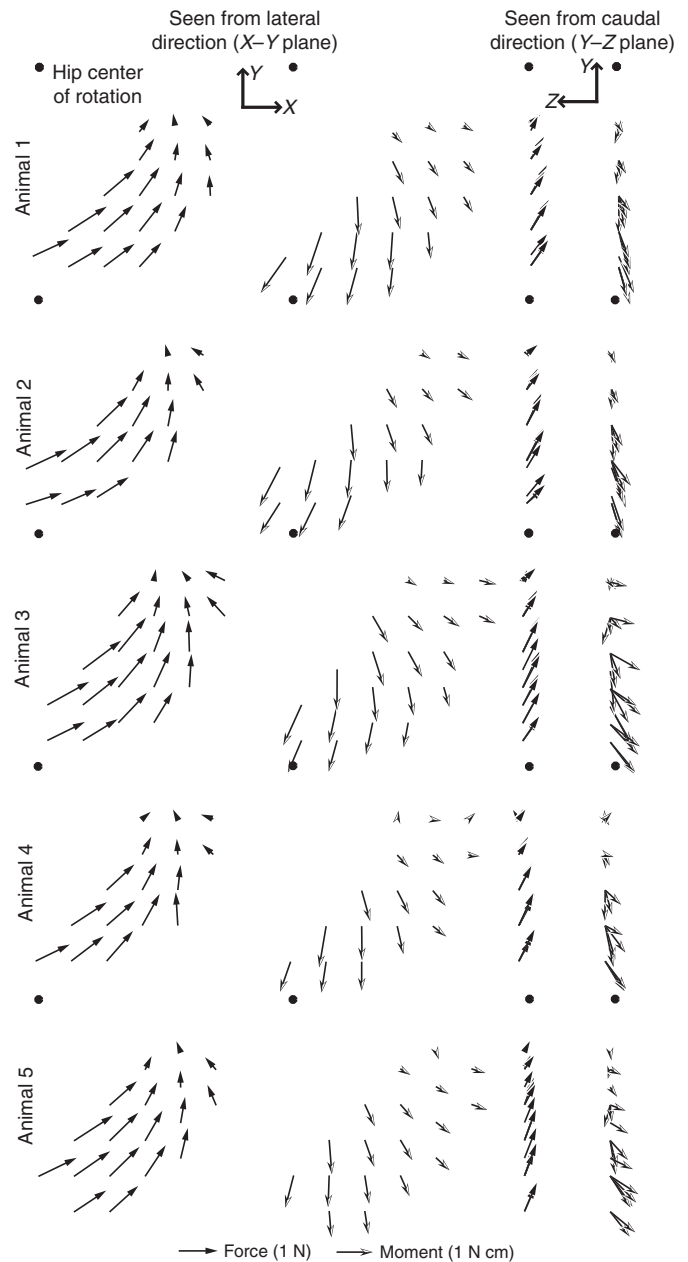


Fig. 3. Force and moment fields evoked by *in situ* stimulation of the gracilis posticus (GRp) for each animal. First two columns show the recorded force (filled arrows) and moment (open arrows) field as seen from the lateral direction ( $X$ - $Y$  plane; see Fig. 1A), and the last two columns show the field as seen from the caudal direction ( $Y$ - $Z$  plane; see Fig. 1A). The position of the hip in each plot is indicated by the filled circle.

minimal dorsal component. Such a caudally directed force suggests that the Bfp acted predominantly as a hip extensor with minimal knee flexion. Fig. 5B shows an example of force and moment fields collected for Bfp with mediolateral rotation either released or restrained, showing that the evoked forces and moments were minimally affected by releasing this degree of freedom.

### Using measured force and moment fields to create muscle models

The force and moment fields illustrated in Figs 3 and 4 reflect the intrinsic force-generating properties of each muscle and the

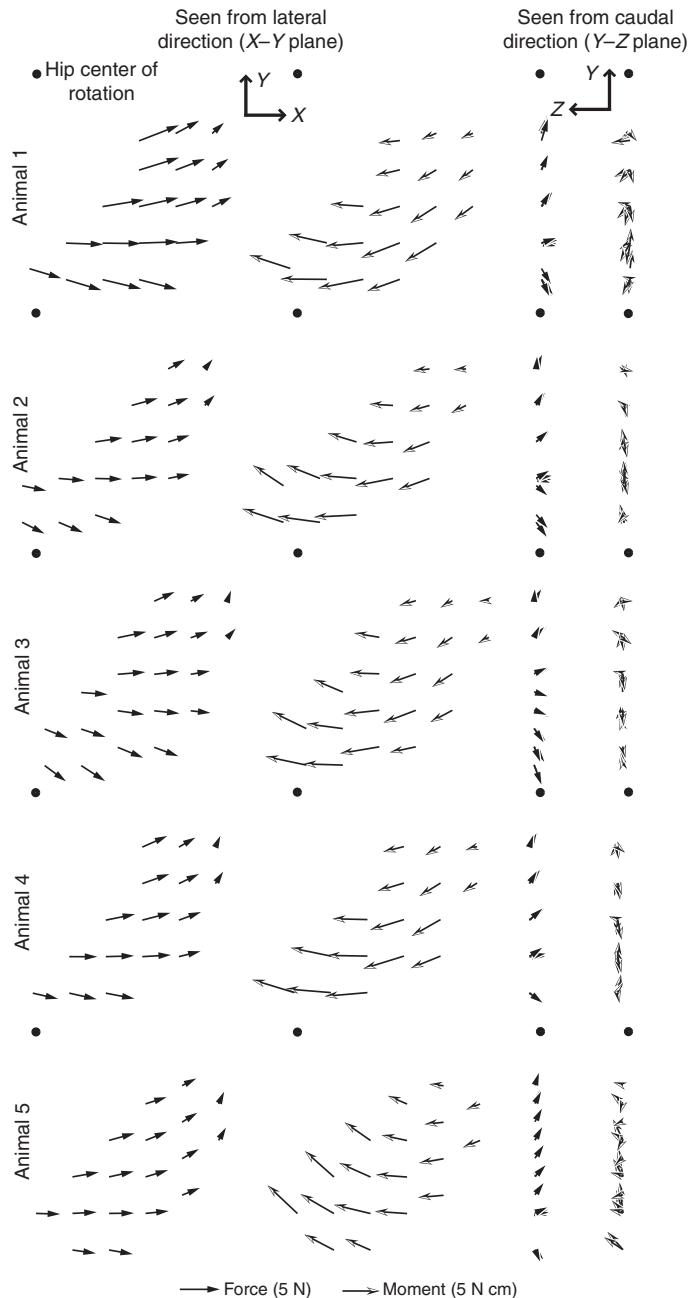


Fig. 4. Force and moment fields evoked by *in situ* stimulation of the BFp. Conventions are the same as in Fig. 3.

attachment of the muscle to the skeleton. We, therefore, attempted to use the observed muscle actions to develop a parameterized muscle model for the GRp and BFp. Each model was described by eight parameters: the optimal muscle length, the maximal force, and the origin and insertion (each a point in three-dimensional space) of each muscle. The parameters that minimized the error between the observed and predicted forces–moment fields were found by optimization. We applied this optimization to the data obtained with the ankle either fully restrained or released, either using the Jacobian with M–P pseudoinverse (restrained analysis) or using the invertible Jacobian without  $z$ -moments (released analysis).

Fig. 6 shows the predictions of the model found for the GRp using the ‘restrained’ method for one animal. In each plot, the thick dark

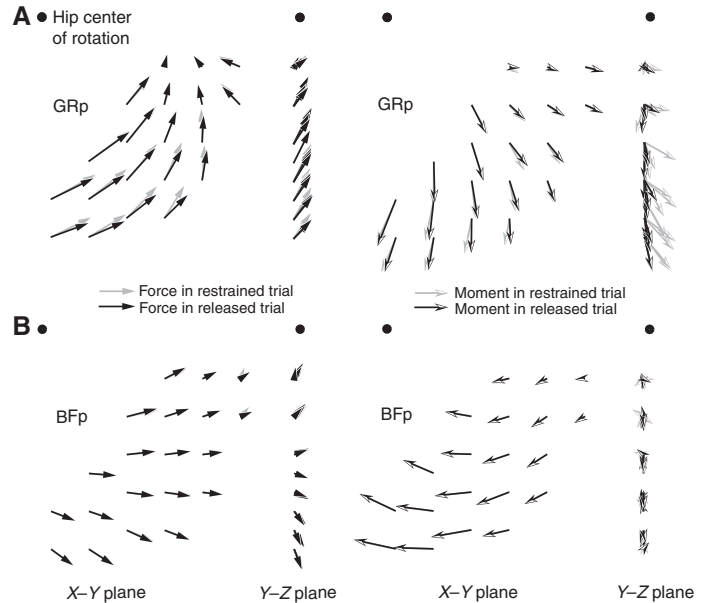


Fig. 5. Comparison of force and moment fields measured in ‘restrained’ trials, in which all movement at the ankle was constrained, and ‘released’ trials in which rotation about the  $Z$ -axis was allowed. (A) Comparison of GRp data collected from animal 3. Gray arrows show the measured force and moment fields in a restrained trial, which is same as data shown in Fig. 3. Black arrows show the measured force and moment fields in a released trial. Note that  $z$ -moments in the released trial are close to zero, because the ankle is allowed to rotate around the  $Z$ -axis. The other forces–moments were only minimally altered between the two restraint conditions. (B) Comparison of BFp data collected from animal 3. Conventions are the same as in A. Note that the force–moment fields for the BFp were nearly identical for released and restrained trials. That is, although both trials are plotted in each figure, at most positions they are indistinguishable.

line indicates the predicted path of the muscle from its origin to its insertion. As can be seen in the plots, the identified model does a very good job of capturing both the forces and moments produced by stimulation of the GRp. The one exception to this good fit is for the  $z$ -moments: the observed response produced a negative  $z$ -moment, whereas the model predicted a positive  $z$ -moment (see Discussion). Because of this deviation in the  $z$ -moment, the  $R^2$  value calculated for this case was quite low ( $R^2=0.62$ ). When this moment was excluded from the calculation, the  $R^2$  value was much higher ( $R^2=0.92$ ). The origins and insertions identified by the model are also consistent with the expected anatomy of the GRp, with an origin near the midline of the pelvis and caudal to the hip, and with an insertion on the tibia partially towards the ankle. Fig. 8A (results from the restrained method are shown by empty symbols) shows the parameters for the origins and insertions found for the GRp in each animal. As can be seen in the figure, these parameters were very similar across animals (s.d. $<0.15$  mm), as might be expected based on the similarity of the force–moment fields shown in Fig. 3. Fig. 8C shows the predicted force–length functions for each animal, suggesting that in each animal the GRp was acting on the ascending portion of its force–length function.

Fig. 7 shows the results of the model found for the BFp using the ‘restrained’ method for the same animal shown in Fig. 3. As was the case for the GRp, the identified model did a very good job of capturing the observed actions of the muscle for both forces and moments. The origin of the model is also consistent with the



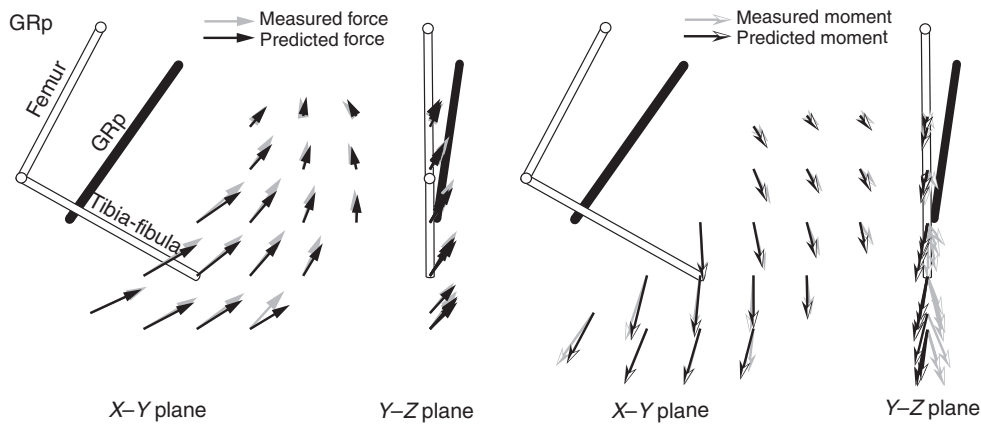


Fig. 6. Example prediction of the force and moment fields evoked by stimulation of the GRp. Gray arrows show the measured force and moments collected from animal 1 (as shown in Fig. 3). Black arrows show the force and moments predicted from the model using the restrained method. The model prediction shows good fit in both forces and moments, but note discrepancy of moments in the Y-Z plane. The estimated muscle path connecting the origin and insertion point are shown as a thick black line in all plots for a single limb configuration. Detailed parameter values are shown in Fig. 8.

expected anatomy of the muscle; it arises from the ischium caudal to the hip. Note the more lateral and dorsal origin of the BFp compared with the GRp. The insertion identified in the model was very close to the knee, consistent with the mainly hip extensor action suggested by the plots in Fig. 4. Fig. 8B (empty symbols) shows the origins and insertions found for the BFp model for each animal, again showing the consistency of the estimated parameters across animals (s.d. < 0.17 mm). Fig. 8D shows that, similar to GRp, the model predicts that the BFp acts along the ascending portion of its force length function.

As described above, we also identified models based on the data sets with ‘released’ trials, in which the rotation around the mediolateral axis was permitted. These models were found using the invertible form of the Jacobian. Fig. 8A,B (filled symbols) shows the parameters found using these models from the released analysis for the GRp and BFp, respectively. Comparison of empty and filled symbols in plots shows that, in general, the model parameters found using the two approaches were very similar to one another.

The models using the ‘released’ method consistently had high  $R^2$  values for both the BFp ( $0.88 \pm 0.02$ ; mean  $\pm$  s.d.) and the GRp ( $0.89 \pm 0.04$ ), consistent with the good fit quality seen in the plots. The models found using the ‘restrained’ method for the BFp also had high  $R^2$  values ( $0.84 \pm 0.06$ ). For the GRp restrained analysis,

the  $R^2$  values were considerably lower ( $0.27 \pm 0.29$ ), primarily because of the consistent offset in the  $z$ -moment as illustrated in Fig. 3. The  $R^2$  values for the GRp increased considerably if this  $z$ -moment was ignored ( $0.85 \pm 0.06$ ). Note that this is a centered  $R^2$  measure, which considers only variations around the mean value in each force–moment dimension. Table 1 summarizes  $R^2$  values for all five animals across the different conditions. Finally, we examined whether the models identified above were overfitting the observed data. We performed an  $n$ -fold cross validation procedure, fitting the data on 80% of the data then evaluating the fit on the remaining 20% of the data. We found that the quality of the fits was only minimally reduced when evaluating such cross validation fits, considering either the force–moment fields predicted using the ‘released’ method for the GRp ( $0.85 \pm 0.03$ ) or BFp ( $0.85 \pm 0.06$ ) or using the ‘restrained’ method for the GRp ( $0.81 \pm 0.06$ , ignoring the  $z$ -moments) and the BFp ( $0.85 \pm 0.03$ , ignoring the  $z$ -moments). This lack of overfitting suggests that the six-dimensional data vectors measured at multiple positions across the workspace place strong constraints on the eight parameters used in the model.

Taken together, the results show that simple muscle models consisting of point origins and point insertions are able to capture the actions of individual muscles in the rat hindlimb very well using either the ‘restrained’ or the ‘released’ procedures. Furthermore, the

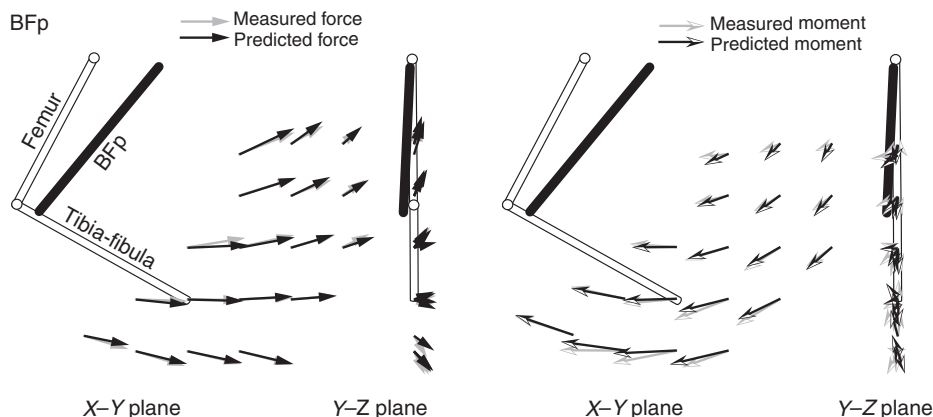


Fig. 7. Example prediction of force and moment fields evoked by BFp stimulation. Conventions are the same as Fig. 6.



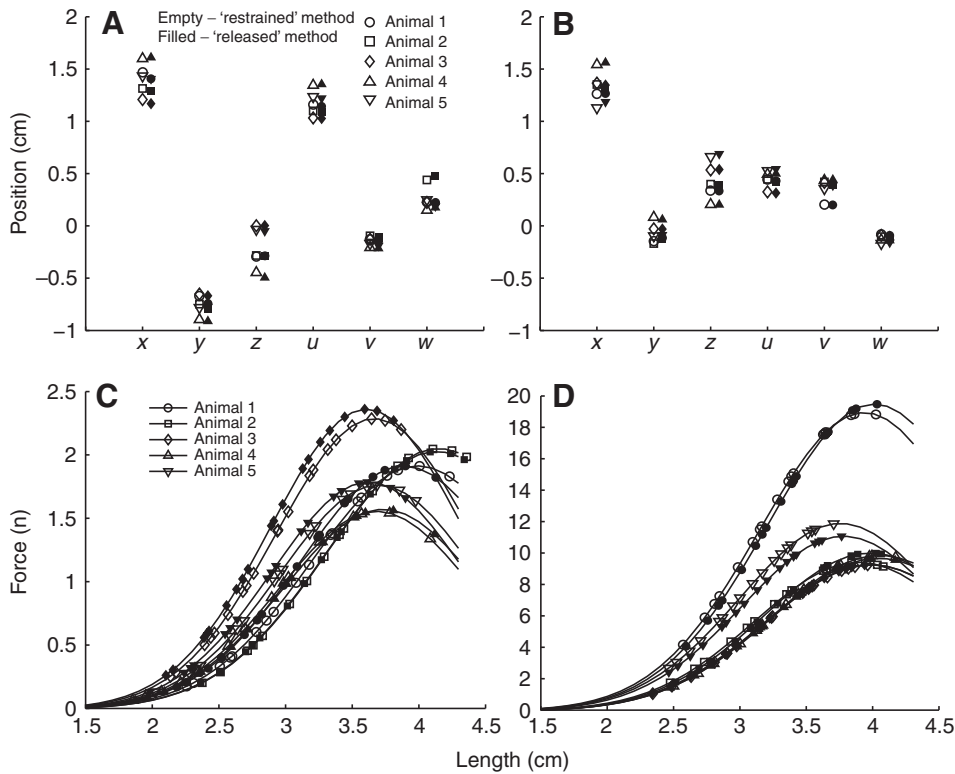


Fig. 8. (A,B) Estimated parameters for the GRp (A) and BFp (B) models for each animal. Parameter values estimated by the restrained and the released method are shown by empty and filled symbols, respectively. The first three parameters are the position of the muscle origin represented by X, Y, Z coordinates and last three are the muscle insertion represented by U, V, W coordinates (coordinates are defined in Fig. 1). (C,D) The force-length relationships of the GRp (C) and the BFp (D) estimated by the model defined in Eqn 1. Lines show the parameterized force-length function and each symbol shows a point on the curve where the force was actually evaluated.

models identified by the two procedures and identified across animals were very similar to one another.

**Comparison with existing musculoskeletal models of the rat hindlimb**

Fig. 9 shows the force and moment fields predicted from the Johnson parameter model (Johnson et al., 2008). As can be seen from the figures, the fields predicted for the GRp from the published parameters were very similar to those found in the present study by

direct stimulation of the GRp (Fig. 3). However, the force-moment field predicted for the BFp is very different from the one observed experimentally using direct stimulation (Fig. 4). In particular, there is a much more prominent knee flexion action predicted for the BFp using the published parameters. This knee flexion action is a consequence of the insertion of the BFp being placed distally along the tibia, reflecting the anatomically distributed insertion of the BFp across the tibia. The results of this comparison suggest that the mechanical action of the BFp as measured here is better predicted

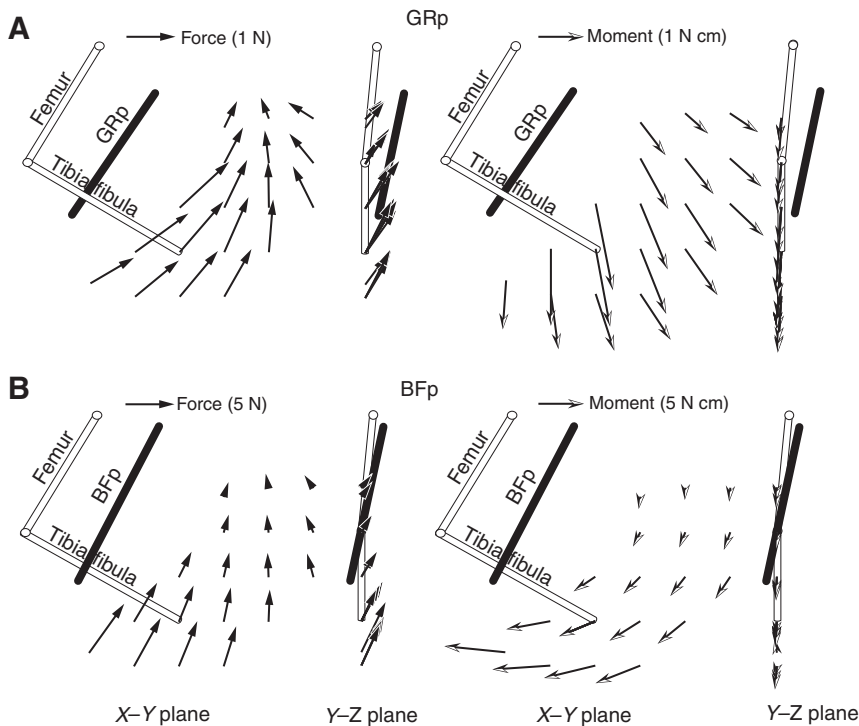


Fig. 9. Prediction of force and moment fields of the GRp (A) and the BFp (B) using anatomical parameters taken from Johnson et al. (Johnson et al., 2008). Conventions are the same as those in Fig. 6. The results are shown in both the lateral (X-Y plane) and the caudal (Y-Z plane) direction.

by a more proximal insertion, such as those shown in Fig. 4 based on direct *in situ* measurements of BFp action, than by a more distal insertion, based on measurements of BFp anatomy.

## DISCUSSION

### Characterization of muscle actions by *in situ* stimulation

As has been suggested in previous work (Giszter et al., 1993; Loeb et al., 2000), we found that the force and moment fields measured here give a succinct representation of muscle actions and their potential contributions to motor control. For instance, although standard characterizations might describe both the GRp and BFp as hip extensor and knee flexors (Greene, 1935), the force and moment fields shown in Figs 3 and 4 illustrate that the actions of these muscles are clearly distinct, not only in terms of their actions in the sagittal plane but also along other degrees of freedom. The description here involving six-dimensional forces and moments provides an especially rich description of muscle actions. It is likely that similar characterizations for other hindlimb muscles (Lawrence et al., 1993; Young et al., 1983) can help to highlight the unique contributions of individual muscles and provide insights into the coordination strategies implemented by the nervous system. The force and moment fields measured in response to stimulation of the GRp were consistent with the actions expected from anatomical inspection of this muscle and were similar to those predicted on the basis of parameters taken from a previous study using anatomical dissections (Johnson et al., 2008). This consistency helps validate the force and moment fields found here and the general approach taken in this study, in addition to helping validate the findings of that previous study. The fields measured in response to the BFp stimulation, in contrast, were more surprising. They reflected a predominant hip extension action, with a relatively small knee flexion contribution. This dominant hip extension action was also confirmed by the proximal insertion of the BFp estimated by our optimization procedures. Straightforward anatomical inspection of BFp suggests that it should produce a more significant knee flexion action than that measured here (Johnson et al., 2008). In fact, the fields predicted by parameters estimated in a previous study, using anatomical inspection, were clearly different from the ones measured here, reflecting the more distal insertion of the BFp estimated in that study. It is unlikely that the mainly hip extension action of the BFp observed here reflected an incomplete activation of all regions of the BFp because with increasing stimulation strength the evoked force magnitude reached a constant level, which did not change with further increases in strength (Fig. 2B). This difference between the insertion of the BFp estimated from anatomical dissection and the insertion estimated from measuring its action illustrates the utility of the approach described here in helping validate and refine musculoskeletal models.

Closer inspection of the structure of the BFp might provide an explanation for how this predominantly hip extensor action is consistent with the anatomy of BFp. Although the insertion of the BFp appears uniformly distributed along the tibia from the knee towards the ankle, reflecting the muscle to expose the medial surface reveals a well defined tendon near the knee into which a large portion of the muscle fibers in the BFp insert. The BFp is also thickest proximally and tapers more distally. Both of these features make it likely that this proximal insertion dominates the action of BFp when the entire muscle is stimulated. This division between a proximal region of the BFp with a well-defined tendon and a more distal region of the muscle with a distributed insertion along the tibia had apparently been recognized by Greene (Greene, 1935), who labeled the more proximal region the biceps femoris posterior and the more diffuse distal region the biceps femoris accessory. However, the

Table 1.  $R^2$  values for muscle force–moment fields for all animals

	Animal 1	Animal 2	Animal 3	Animal 4	Animal 5
BFp, released	0.89	0.89	0.90	0.85	0.88
GRp, released	0.93	0.94	0.87	0.85	0.88
BFp, restrained	0.87	0.87	0.90	0.79	0.76
GRp, restrained	0.62	0.47	−0.01	0.29	−0.03
BFp, restrained (without z-moment)	0.91	0.89	0.90	0.85	0.87
GRp, restrained (without z-moment)	0.92	0.91	0.80	0.81	0.81

BFp, posterior head of biceps femoris muscle; GRp, gracilis posticus muscle.

exact division between these two regions is not obvious from simple inspection (Nicolopoulos-Stournaras and Iles, 1984; Parsons, 1896). In the cat, the BFp has been suggested to be divided into three compartments defined by separate innervation territories (Carrasco and English, 1999; Chanaud et al., 1991) and the divisions described here in the rat might similarly correspond to different compartments. Further experiments stimulating individual nerve branches to the BFp or partially cutting its insertion might help clarify the actions of different regions of the BFp.

It should also be noted that in order to isolate the muscles stimulated here we had to perform extensive dissections of the hindlimb. These dissections obviously interrupted connective tissue interactions between muscles, for instance between the BFp and the semitendinosus, the BFa and BFp, and the GRa and GRp, all of which have close adhesions. Similarly, in order to place bone screws on the distal tibia we interrupted the fascial sheath of the lateral limb. The importance of these intermuscular connections is not fully understood. In some circumstances, these interactions have been shown to significantly affect the forces produced by stimulation of individual muscles (Huijing and Baan, 2001; Hyde et al., 1999). During more physiological conditions, however, they have not been found to make a substantial difference in the force measured (Maas and Sandercock, 2008; Sandercock, 2005). In addition, some fascial sheets may need to be tensed by active muscles in order to transmit force normally. To characterize such effects, individual muscle actions might have to be studied on top of the background activity of other muscles. Future experiments might measure the force and moment fields with and without such connective tissue interactions or with and without other muscles pre-activated to gain a better understanding of the consequences of these nontraditional pathways of force transmission.

### Developing musculoskeletal muscle models based on *in situ* measurements of muscle actions

Beyond its use in validating and refining musculoskeletal models, we also demonstrated that the approach described here can be used directly to specify the parameters of a muscle model. This approach is related to previous work in which moment arms were estimated at single postures based on forces applied to tendons in cadavers (Lee et al., 2008; Pearlman et al., 2004; Santos and Valero-Cuevas, 2003; Valero-Cuevas et al., 2003; Valero-Cuevas et al., 2000) and in which planar force fields were used to find functional approximations of moment arm variations across the workspace (Loeb et al., 2000). The present study extends that work to use the forces and moments to specify a simple anatomical model of muscle action. We showed that a simple model of muscle action, based on a single origin and insertion along with the optimal length and force of the muscle, was able to describe the actions of both the GRp and

the BFp very well. The good fits for the GRp with this model were consistent with the relatively circumscribed origin and insertion of this muscle, suggesting the validity of the approach used here.

However, we were surprised by the ability of this simple model, with a single origin and insertion, to explain the actions of the complex muscle BFp. We expected this muscle to show the limitations of this simple model structure, showing how the measurements from direct muscle stimulation could be used to justify the creation of distinct subregions and to specify their placement. As discussed above, it might be that this good fit reflected the dominant action of the more proximal tendon of the BFp, allowing it to be well described with a single insertion. Whether other complex muscles can be as well described with a single origin and insertion will require further experiments.

Ultimately, whether a complex muscle such as the BFp should be represented by a single insertion or multiple insertions and where those insertions should be placed depends not only on being able to explain the mechanical action of the muscle but also on being able to explain the activation of the muscle by the nervous system. For example, even though the present experiments suggest that we could explain the mechanical action of the entirety of the BFp by a single insertion point, it is probable that the nervous system does not activate the BFp homogeneously. Previous work in the adult cat (Chanaud and Macpherson, 1991; Pratt et al., 1991) and our own work in the neonatal rat (Klein et al., 2010) have shown that regions of the BFp are activated differentially in behaviors such as locomotion and posture. Obviously, the mechanical consequences of this differential activation cannot be explained using a musculoskeletal model of BFp with a single origin and insertion. Such considerations emphasize the iterative process of refinement and elaboration involved in creating musculoskeletal models, requiring a combination of both biomechanical and neurophysiological studies.

The results of this study were mainly focused on estimating the origins and insertions of the GRp and the BFp, based on the structure of the measured force–moment fields. These origins and insertions determine how the direction of the six-dimensional vector measured at the ankle varies across limb configurations, which is a crucial aspect of all musculoskeletal models. Our models also included estimates of the force–length properties of each muscle, as defined by the maximal force and optimal muscle length parameters. These properties influence the magnitude of the vector at each limb configuration but do not affect the direction of the predicted vector. The model of force generation used in this study only included parameters defining the maximal force and optimal length of each muscle and did not include a parameter for the resting tendon length (Zajac, 1989). Because we only made isometric measurements in these experiments and because these muscles are likely to be acting mainly on the ascending portion of their force–length functions (see Fig. 8, and from predictions from Johnson model parameters), including this extra parameter is not expected to increase the fit quality of the identified models, consistent with the very good fits shown here. For other muscles, such as distal muscles with long tendons or muscles operating on both the ascending and descending portion of the force–length function, it should be possible to estimate the tendon length and increase the quality of the observed fits by including this parameter. Note, however, that because of the independence between force–moment direction and intrinsic force generation described above, this simplification would not be expected to alter the estimated origin and insertion of each muscle. Similarly, although equations other than the one used here could be used to characterize the force–length relationship of muscle, it is unlikely that their

use would affect the estimated anatomical parameters. Further experiments in which muscle actions are characterized dynamically or across a wider range of conditions might make it possible to estimate these force-generating properties of muscles more completely.

Note also that although the experiments described here involved extensive dissections to isolate individual muscles, other less invasive methods of estimating muscle actions have been developed (Kutch et al., 2010). Such less invasive methods might be used in combination with the computational analyses described in this study to construct musculoskeletal models.

#### Future directions and conclusions

The present study demonstrates the potential utility of *in situ* measurements of muscle actions to validate and develop musculoskeletal muscle models. However, it is important to point out several limitations of the present study. First, the measurements made here are obviously subject to experimental error. This error arises for a number of reasons, including imperfect mechanical isolation of the hip, muscle fatigue both within and between trials, and idealized kinematic models of joints. For instance, the  $z$ -moments observed for the GRp could not be explained with the models considered here. In fact, the negative  $z$ -moments observed from stimulation should be impossible for any muscle if the hip was completely mechanically fixed. Obtaining ideal mechanical fixation is clearly difficult because of the considerable internal flexibility in the sacrum and pelvis: despite placing bone screws on the contralateral pelvis and on the rostral ipsilateral pelvis, there could still be some movement of the hip during muscle stimulation because of internal flexion of the pelvis. We were unable to restrain the skeleton further without interrupting the insertion of the BFp on the pelvis. Although this imperfect fixation can apparently alter the measured actions of muscles, it is important to note that these effects did not substantially affect the models identified in these experiments: if we excluded the  $z$ -moment from the optimizations, the anatomical parameters estimated were affected only minimally. Using more accurate joint models and tracking the exact skeletal configuration at each limb configuration would also potentially increase the accuracy of models developed using the methods described here.

The ‘top down’ approach described here to estimate the static properties of muscles might, in principle, also be used to estimate the dynamic properties of muscles, taking measurements of the behaviour of the intact muscle when the limb is being moved through a variety of trajectories, then using those measurements to estimate dynamic properties of muscles. Whether the increased complexity of such experiments would still provide useful estimates of these properties or whether straightforward morphometric measurements of muscles would be simpler and more accurate is not clear at present. Regardless of whether such experiments might be useful for estimating musculoskeletal models, it is clear that they would be useful for validating models created from other procedures. Evaluating the utility of this approach for dynamic properties of muscles will require further experiments.

It will be interesting in future work to evaluate the sensitivity to these sources of error of the models identified using the top down approach of this study. Whether or not the consequences of these measurement errors are greater in this top down approach than they are in more traditional ‘bottom-up’ approaches based on anatomical measurements (Santos et al., 2009), it seems clear that combining the information from both approaches can be a useful way to create and refine complex musculoskeletal models.



## LIST OF SYMBOLS AND ABBREVIATIONS

BFP	posterior head of biceps femoris muscle
$\mathbf{d}$	the eight-dimensional vector of muscle model parameters
$\mathbf{F}_m$	(3×1) vector of forces
$f_{\max}$	maximal force
GRp	gracilis posticus muscle
$J_a$	(6×5) Jacobian relating muscle force–moments measured at the ankle to joint torques
$\bar{J}_a$	(5×5) Jacobian for the ‘released’ method
$J_m$	(3×5) Jacobian relating muscle force to joint torques
$l$	muscle length
$l_o$	optimal muscle length
$\boldsymbol{\tau}_a$	(5×1) vector of joint torques needed to produce $\boldsymbol{\Psi}_a$ at the endpoint
$\boldsymbol{\tau}_m$	(5×1) vector of joint torques created by the muscle force
$\boldsymbol{\Psi}_a$	(6×1) vector of forces and moments measured at the ankle
$\hat{\boldsymbol{\Psi}}_a$	(5×1) reduced vector of forces and moments for the ‘released’ method
$\hat{\boldsymbol{\Psi}}_i(\mathbf{d})$	ankle force and moments predicted for the $i$ th configuration

## ACKNOWLEDGEMENTS

We are grateful to Brian Macrie and Julian Klosowiak for helping with pilot experiments and Will Johnson for help with the rat hindlimb model. This research was supported by NIH NIAMS R01AR053608 and NIH NINDS R21NS061208 to M.C.T. and by the Canada Research Chairs Program, NSERC, and Peter Wall Institute for Advanced Studies to D.K.P. Deposited in PMC for release after 12 months.

## REFERENCES

- Brown, I. E. and Loeb, G. E.** (2000). A reductionist approach to creating and using neuromusculoskeletal models. In *Biomechanics and Neural Control of Posture and Movement* (ed. J. M. Winters and P. E. Crago), pp. 148–163. New York: Springer-Verlag.
- Burkholder, T. J. and Nichols, T. R.** (2004). Three-dimensional model of the feline hindlimb. *J. Morphol.* **261**, 118–129.
- Carrasco, D. and English, A.** (1999). Mechanical actions of compartments of the cat hamstring muscle, biceps femoris. *Prog. Brain Res.* **123**, 397–403.
- Chadwick, E., Blana, D., van den Bogert, A. and Kirsch, R.** (2008). A real-time, 3D musculoskeletal model for dynamic simulation of arm movements. *IEEE Trans. Biomed. Eng.* **56**, 941–948.
- Chanaud, C. and Macpherson, J.** (1991). Functionally complex muscles of the cat hindlimb. III. Differential activation within biceps femoris during postural perturbations. *Exp. Brain Res.* **85**, 271–280.
- Chanaud, C., Pratt, C. and Loeb, G.** (1991). Functionally complex muscles of the cat hindlimb. II. Mechanical and architectural heterogeneity within the biceps femoris. *Exp. Brain Res.* **85**, 257–270.
- Delp, S. L. and Loan, J. P.** (1995). A graphics-based software system to develop and analyze models of musculoskeletal structures. *Comput. Biol. Med.* **25**, 21–34.
- Delp, S., Anderson, F., Arnold, A., Loan, P., Habib, A., John, C., Guendelman, E. and Thelen, D.** (2007). OpenSim: Open-source software to create and analyze dynamic simulations of movement. *IEEE Trans. Biomed. Eng.* **54**, 1940–1950.
- Eng, C. H., Smallwood, L. H., Rainiero, M. P., Lahey, M., Ward, S. R. and Lieber, R. L.** (2008). Scaling of muscle architecture and fiber types in the rat hindlimb. *J. Exp. Biol.* **211**, 2336–2345.
- Gillis, G. B. and Biewener, A. A.** (2001). Hindlimb muscle function in relation to speed and gait: *in vivo* patterns of strain and activation in a hip and knee extensor of the rat (*Rattus norvegicus*). *J. Exp. Biol.* **204**, 2717–2731.
- Giszter, S. F., Mussa-Ivaldi, F. A. and Bizzi, E.** (1993). Convergent force fields organized in the frog’s spinal cord. *J. Neurosci.* **13**, 467–491.
- Golub, G. H. and van Loan, C. F.** (1996). *Matrix Computations*. Baltimore: Johns Hopkins University Press.
- Gordon, A. M., Huxley, A. F. and Julian, F. J.** (1966). The variation in isometric tension with sarcomere length in vertebrate muscle fibres. *J. Physiol.* **184**, 170–192.
- Greene E. C.** (1935). Anatomy of the rat. *Trans. Am. Philos. Soc.* **V27**.
- Holzbaumer, K. R. S., Murray, W. M. and Delp, S. L.** (2005). A model of the upper extremity for simulating musculoskeletal surgery and analyzing neuromuscular control. *Ann. Biomed. Eng.* **33**, 829–840.
- Huijing, P. A. and Baan, G. C.** (2001). Myofascial force transmission causes interaction between adjacent muscles and connective tissue: effects of blunt dissection and compartmental fasciotomy on length force characteristics of rat extensor digitorum longus muscle. *Arch. Physiol. Biochem.* **109**, 97–109.
- Hyde, L., Burkholder, T. and Nichols, T.** (1999). Reflex action of the hamstrings muscles at the feline ankle mediated by the crural fascia. *Soc. Neurosci. Abst.* **25**, 1151.
- Johnson, W. L., Jindrich, D. L., Roy, R. R. and Reggie Edgerton, V.** (2008). A three-dimensional model of the rat hindlimb: musculoskeletal geometry and muscle moment arms. *J. Biomech.* **41**, 610–619.
- Kargo, W. J. and Rome, L. C.** (2002). Functional morphology of proximal hindlimb muscles in the frog *Rana pipiens*. *J. Exp. Biol.* **205**, 1987–2004.
- Kargo, W. J., Nelson, F. and Rome, L. C.** (2002). Jumping in frogs: assessing the design of the skeletal system by anatomically realistic modeling and forward dynamic simulation. *J. Exp. Biol.* **205**, 1683–1702.
- Klein, D. A., Patino, A. and Tresch, M. C.** (2010). Flexibility of motor pattern generation across stimulation conditions by the neonatal rat spinal cord. *J. Neurophysiol.* **103**, 1580–1590.
- Kutch, J. J., Kuo, A. D. and Rymer, W. Z.** (2010). Extraction of individual muscle mechanical action from endpoint force. *J. Neurophysiol.* **103**, 3535–3546.
- Lawrence, J. H., 3rd, Nichols, T. R. and English, A. W.** (1993). Cat hindlimb muscles exert substantial torques outside the sagittal plane. *J. Neurophysiol.* **69**, 282–285.
- Lee, S. W., Chen, H., Towles, J. D. and Kamper, D. G.** (2008). Estimation of the effective static moment arms of the tendons in the index finger extensor mechanism. *J. Biomech.* **41**, 1567–1573.
- Loeb, E. P., Giszter, S. F., Saltiel, P., Bizzi, E. and Mussa-Ivaldi, F. A.** (2000). Output units of motor behavior: an experimental and modeling study. *J. Cogn. Neurosci.* **12**, 78–97.
- Maas, H. and Sandercock, T. G.** (2008). Are skeletal muscles independent actuators? Force transmission from soleus muscle in the cat. *J. App. Physiol.* **104**, 1557–1567.
- McKay, J. L., Burkholder, T. J. and Ting, L. H.** (2007). Biomechanical capabilities influence postural control strategies in the cat hindlimb. *J. Biomech.* **40**, 2254–2260.
- Murray, R. Li, Z. and Sastry, S. S.** (1994). *A Mathematical Introduction to Robotic Manipulation*. London: CRC Press.
- Mussa-Ivaldi, F. A. and Hogan, N.** (1991). Integrable solutions of kinematic redundancy via impedance control. *Int. J. Robotics Res.* **10**, 481–491.
- Nicolopoulos-Stourmaras, S. and Iles, J. F.** (1984). Hindlimb muscle activity during locomotion in the rat (*Rattus norvegicus*) (Rodentia: Muridae). *J. Zool.* **203**, 427–440.
- Nishikawa, K., Biewener, A. A., Aerts, P., Ahn, A. N., Chiel, H. J., Daley, M. A. and Daniel, T. L., Full, R. J., Hale, M. E., Hedrick, T. L. et al.** (2007). Neuromechanics: an integrative approach for understanding motor control. *Integr. Comp. Biol.* **47**, 16–54.
- Parsons, F. G.** (1896). 4. Myology of rodents. Part II. An account of the myology of the Myomorpha, together with a comparison of the muscles of the various suborders of rodents. *Proc. Zool. Soc.* **64**, 159–192.
- Pearlman, J. L., Roach, S. S. and Valero-Cuevas, F. J.** (2004). The fundamental thumb-tip force vectors produced by the muscles of the thumb. *J. Orthop. Res.* **22**, 306–312.
- Pfeifer, R., Lungarella, M. and Iida, F.** (2007). Self-organization, embodiment, and biologically inspired robotics. *Science* **318**, 1088–1093.
- Pratt, C., Chanaud, C. and Loeb, G.** (1991). Functionally complex muscles of the cat hindlimb. IV. Intramuscular distribution of movement command signals and cutaneous reflexes in broad, bifunctional thigh muscles. *Exp. Brain Res.* **85**, 281–299.
- Rassier, D. E., MacIntosh, B. R. and Herzog, W.** (1999). Length dependence of active force production in skeletal muscle. *J. Appl. Physiol.* **86**, 1445–1457.
- Sandercock, T. G.** (2005). Summation of motor unit force in passive and active muscle. *Exerc. Sport Sci. Rev.* **33**, 76–83.
- Santos, V. J. and Valero-Cuevas, F. J.** (2003). Anatomical variability naturally leads to multimodal distributions of Denavit-Hartenberg parameters for the human thumb, pp. 17–21. *Proc. 25th Ann. Intl Conf. IEEE EMBS*.
- Santos, V. J., Bustamante, C. D. and Valero-Cuevas, F. J.** (2009). Improving the fitness of high-dimensional biomechanical models via data-driven stochastic exploration. *IEEE Trans. Biomed. Eng.* **56**, 552–564.
- Sueda, S., Kaufman, A. and Pai, D. K.** (2008). Musculotendon simulation for hand animation. *Proc. ACM SIGGRAPH 2008 papers*. **27**, 83.
- Teran, J., Blemker, S., Hing, V. and Fedkiw, R.** (2003). Finite volume methods for the simulation of skeletal muscle. *Proc. ACM SIGGRAPH/Eurographics Symposium on Computer Animation* 68–74.
- Topp, E. L. and Rosen, J. M.** (1990). An interactive graphics-based model of the lower extremity to study orthopaedic surgical procedures. *IEEE Trans. Biomed. Eng.* **37**, 757–767.
- Tresch, M. C. and Bizzi, E.** (1999). Responses to spinal microstimulation in the chronically spinalized rat and their relationship to spinal systems activated by low threshold cutaneous stimulation. *Exp. Brain Res.* **129**, 401–416.
- Tresch, M. C., Klein, D. A., Yeo, S. H., Mullens, C. H., Sandercock, T. G. and Pai, D. K.** (2010). Understanding complex muscles in the rat hindlimb: activations and actions. *Proc. 32th IEEE Eng. Med. and Biol. Soc.* Buenos Aires, Argentina.
- Valero-Cuevas, F. J., Towles, J. D. and Hentz, V. R.** (2000). Quantification of fingertip force reduction in the forefinger following simulated paralysis of extensor and intrinsic muscles. *J. Biomech.* **33**, 1601–1609.
- Valero-Cuevas, F. J., Johanson, M. E. and Towles, J. D.** (2003). Towards a realistic biomechanical model of the thumb: the choice of kinematic description may be more critical than the solution method or the variability/uncertainty of musculoskeletal parameters. *J. Biomech.* **36**, 1019–1030.
- Valero-Cuevas, F. J., Anand, V. V., Saxena, A. and Lipson, H.** (2007a). Beyond parameter estimation: Extending biomechanical modeling by the explicit exploration of model topology. *IEEE Trans. Biomed. Eng.* **54**, 1951–1964.
- Valero-Cuevas, F. J., Yi, J., Brown, D., McNamara, R. V., Paul, C. and Lipson, H.** (2007b). The tendon network of the fingers performs anatomical computation at a macroscopic scale. *IEEE Trans. Biomed. Eng.* **54**, 1161–1166.
- Valero-Cuevas, F. J., Hoffmann, H. M., Kurse, M. U., Kutch, J. J. and Theodorou, E. A.** (2009). Computational models for neuromuscular function. *IEEE Rev. Biomed. Eng.* **2**, 110–135.
- Young, R. P., Scott, S. H. and Loeb, G. E.** (1983). The distal hindlimb musculature of the cat: multiaxis moment arms at the ankle joint. *Exp. Brain Res.* **96**, 141–151.
- Zajac, F. E.** (1989). Muscle and tendon: properties, models, scaling, and application to biomechanics and motor control. *Crit. Rev. Biomed. Eng.* **17**, 359–411.